Chemical Technology
ISSN: 0974-7443

Chemical Technology: An Indian Journal

**Research** | Vol 12 Iss 1

# Urchin-Flower like Hierarchical LaNiO3 Spheres: Structural Characteristics and Photocatalytic Activity

**Song W*, Ma S, Sun L, Yang Y, Sun J and Liu P**

College of Chemistry and Chemical Engineering, Qiqihar University Qiqihar, P.R. China

***Corresponding author:** Song W, College of Chemistry and Chemical Engineering, Qiqihar University Qiqihar, P.R. China, Tel: 0086-452-2738469; E-mail: qdsongweiming@163.com

**Received:** January 06, 2017; **Accepted:** June 24, 2017; **Published:** June 28, 2017

## Abstract

**Urchin-flowerlike hierarchical $LaNiO_3$ spheres were synthesized by a modified coprecipitation method from vesicle solutions. The $LaNiO_3$ spheres' structure and catalytic activity were elaborately studied by varying the mole ratio of La and Ni. Both samples were characterized by XRD, SEM, TEM and XPS, the results revealed a variety of urchin-flowerlike hierarchical $LaNiO_3$ spheres with different La/Ni molar ratios (n(La): n (Ni)=1:1, 2:1, 3:1, 4:1) were prepared by self-assembly method, and all the catalysts provided typical diffraction patterns for the $LaNiO_3$ rhombohedral structure characteristics. Urchin-flowerlike hierarchical $LaNiO_3^{-3}$ spheres (~20 µm to 30 µm diameter) shows a typical urchin-flowerlike hierarchical sphere structure, which was composed of ~100-nm-thickultrathin sheets. The $LaNiO_3^{-3}$ has a better morphology, crystal configuration, photocatalytic activity (95.63%) for RB under ultraviolet light.**

***Keywords:** Urchin-flowerlike; LaNiO3 spheres; Hierarchical*

## Introduction

Organic compounds are widely dispersed and likely to occur as environmental hazards in water. Among different organic pollutants, dyes have been designated as priority pollutants by many countries, because of their acute toxicity and long persistence. Thus, they must be degraded to below environmentally accepted levels before safe disposal to public health. Three dimensional nanomaterials attract much attention in recent years. Preparing three dimensional nanomaterials with specific surface area, good chemical activity and adsorption selectivity properties.

Three-dimensional metal oxide micro-/nanostructures have received much attention because of their potential applications in the fields of catalysis, electrical, water treatment. The self-assembly of inorganic nanostructured building blocks into 3D ordered hierarchical nanostructures is fascinating because variation of the arrangements of the building blocks provides a method to tune the properties of the material. Rare earth nanomaterials [1-3] with specific surface area, good chemical activity and adsorption selectivity excellent properties has potential applications in fluorescent, hydrogen storage, catalysis and other fields [4].

In recent years, many synthesis efforts have focused on using vesicles with special structures and their unique self-assembling properties as templates to prepare novel structural materials. Zou YC had fabricated $BaZrO_3$ hollow microspheres by a simple reflux method [5]. Shanmugasundaram A had fabricated hierarchical mesoporous $In_2O_3$ with enhanced CO sensing and photocatalytic performance [6].

The aim of this work was to synthesize urchin-flowerlike [7] hierarchical $LaNiO_3$ [8-10] spheres by a modified coprecipitation method from ultrahigh dilute (vesicle) solutions [11,12], and to study their structural characteristics. The $LaNiO_3$ spheres' structure and catalytic activity were elaborately studied by varying the mole ratio of La and Ni. This method is attractive because of its relative simplicity, environmental friendliness, affordability, and suitability for large-scale production. Various characterization techniques, namely scanning electron microscopy (SEM), X-ray diffraction (XRD), transmission electron microscopy (TEM), and temperature-programmed reduction (TPR), were used to characterize the physical and chemical properties of the synthesized materials [13-16].

## Experimental

### Sample preparation

Materials. All chemicals were of analytical grade and were used without further purification. Lanthanum nitrate ($La(NO_3)_3 \cdot 6H_2O$), nickel nitrate ($Ni(NO_3)_2 \cdot 6H_2O$), NaOH, hexadecyl trimethyl ammonium bromide (CTAB), and sodium dodecyl benzene sulfonate (SDBS) were purchased from Tianjin Kemiou Chemical Reagent Co., Ltd.

Synthesis of urchin-flowerlike hierarchical $LaNiO_3$ spheres. A solution of vesicles was obtained by dissolving surfactants CTAB and SDBS (CTAB: SDBS=1:2 molar ratio; 0.028 mol/L surfactant) in twice-distilled water at 30°C for 18 h. The urchin-flowerlike hierarchical $LaNiO_3$ spheres were synthesized by a modified coprecipitation method from an ultrahigh dilute (vesicle) solution. 0.649 g $La(NO_3)_3 \cdot 6H_2O$ and $Ni(NO_3)_2 \cdot 6H_2O$ (n(La):n(Ni)=1:1, 2:1, 3:1, 4:1) were dissolved in 15 and 10 mL of deionized water, respectively. These solutions were added to 75 mL of the vesicle solution. A precipitate was obtained by the drop wise addition of NaOH solution until the solution pH reached 8.5. The resultant light-blue slurry was decanted, filtered, and washed several times with twice-distilled water to remove anion impurities. The collected precipitate was oven-dried at 80 K for 12 h, crushed using an agate mortar, and then calcined at 750 K for 5 h at 5 K $min^{-1}$ in air to obtain the urchin-flowerlike hierarchical $LaNiO_3$ -1 ($LaNiO_3^{-2}$, $LaNiO_3^{-3}$, $LaNiO^{-4}$) spheres (SCHEME 1).

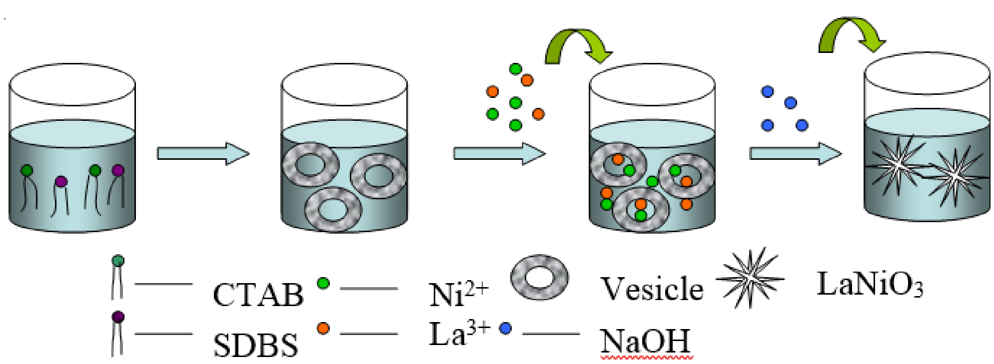


SCHEME 1. **Procedure for the synthesis of urchin-flowerlike hierarchical $LaNiO_3$ spheres.**

### Material characterization

The morphology was studied by SEM on a JEOL JSM-6360 electron microscope. TEM was performed with an FEI-TECHNI-G2 instrument at an operating voltage of 200 kV. XRD analysis was performed using a MAC Science MXP18 diffractometer with Cu K$\alpha_1$ radiation (λ=1.5405 Å) at 40 kV and 30 mA for 2θ from 10-80°C at 10°C/min to identify the amorphous structure. The surface composition and surface electronic state were analyzed by X-ray photoelectron spectroscopy (XPS) using a Kratos Axis Ultra DLD instrument at 160 eV pass energy. Al Kα radiation was used to excite the photoelectrons. The binding energy value of each element was corrected using C 1s=284.6 eV as a reference. TPR experiments were carried out in a fixed-bed reactor. Sample (50 mg) was loaded, and 4.2% $H_2/N_2$ reduction gas (30 mL/min) was introduced. The temperature of the reactor was raised linearly from room temperature to 850°C at 10°C/min using a temperature controller. For the catalysis study, 60 mL of 30 mg/L Reactive Brilliant Red (RB) solution was taken in a beaker and 20 mg of $LaNiO_3$ was added to it. The resulting solution was stirred while keeping away from the light source and then the solution was centrifuged to separate the $LaNiO_3$.

## Results and Discussion

### X-ray diffraction analysis

XRD measurements were performed to identify the chemical states of the urchin-flowerlike hierarchical $LaNiO_3$ spheres. FIG. 1 gives the XRD spectrum of the $LaNiO_3$ spheres. Several significant diffraction peaks appeared at 2θ＝23.32°, 32.83°, 39.38°, 47.15°, 52.04°, 52.61°, 58.64°, 68.96°, 78.89° and the resulting diffraction peaks can be indexed to characteristic diffractions from (101), (110), (021), (202), (211), (113), (122), (220), (312) of $LaNiO_3$ (JCPDF No. 034-1028) [17,18]. The sample was typically of a $LaNiO_3$ perovskite structure with a rhombohedral crystal system [19]. Nanocrystalline $La_2O_3$ was synthesized by a modified coprecipitation method from ultrahigh dilute (vesicle) solution, using $La(NO_3)_3 \cdot 6H_2O$ as raw material and NaOH as precipitant. Several significant diffraction peaks appeared at 2θ＝26.61°, 29.08°, 29.95°, 48.92° and the resulting diffraction peaks can be indexed to characteristic diffractions from (100), (002), (021), (101), (110) of $La_2O_3$ (JCPDF No. 005-0602). These results indicate that the chemical state of the LaNiO3 is the same in the support.

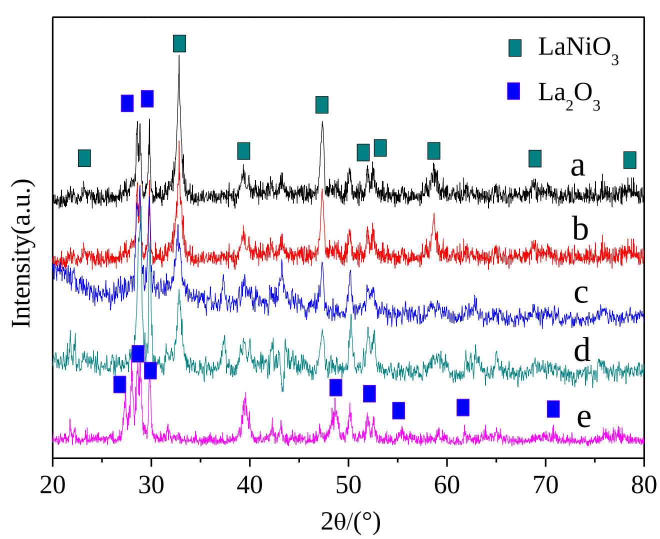


FIG. 1. **XRD spectra of urchin-flowerlike hierarchical $LaNiO_3$ spheres a: n(La/Ni)=1:1, b: n(La/Ni)=2:1, c: n(La/Ni)=3:1, d: n(La/Ni)=4:1.**

### Scanning electron microscopy analysis

The urchin-flowerlike hierarchical $LaNiO_3$ spheres were synthesized successfully by a modified coprecipitation method from ultrahigh dilute (vesicle) solution. Various $LaNiO_3$ microstructures were obtained at different magnifications as shown in FIG. 2. The SEM micrographs in FIG. 2a show that the $LaNiO_3^{-3}$ spheres diameters are ~20 µm to 30 µm. FIG. 2b shows a single $LaNiO_3^{-3}$ spheres with a typical sea urchin-flowerlike hierarchical structure; having a common centre. FIG. 2c shows regular multilayer nanoribbons with spiny three-dimensional structure. The $LaNiO_3^{-3}$ spheres are composed of ultrathin nanosheets (~100 nm), which self-assemble in orderly rows, termed nanoribbons (FIG. 2d).

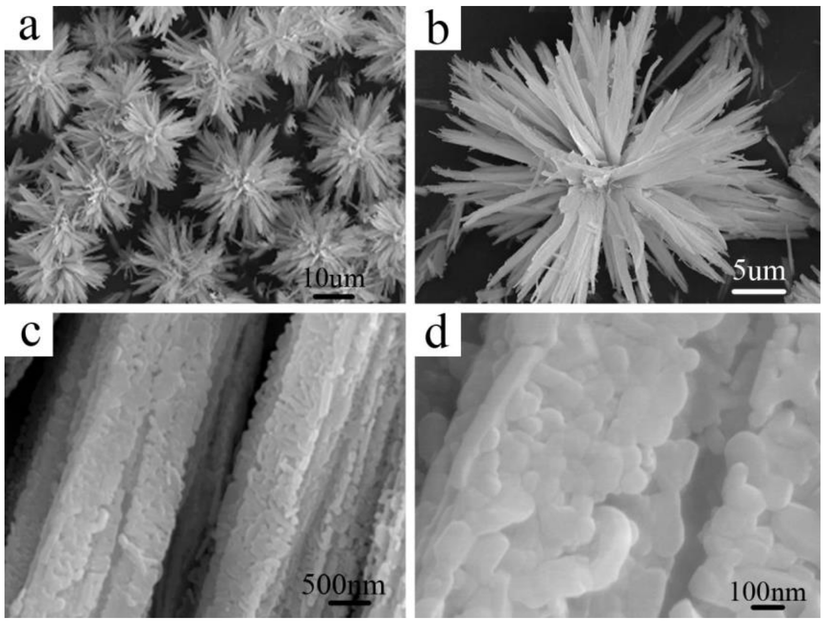


FIG. 2. **SEM micrographs of urchin-flowerlike hierarchical $LaNiO_3$-3 spheres**

### Transmission electron microscopy analysis

TEM and high-resolution TEM (HRTEM) were used to study the urchin-flowerlike hierarchical $LaNiO_3$ spheres structure. FIG. 3 shows the TEM micrographs of the $LaNiO_3$ spheres. Many of the $LaNiO_3$ spheres are less than 200 nm in diameter (FIG. 3a). FIG. 3b (high magnification) displays the well-defined lattice fringes of the d=0.275 nm (110) crystal plane of one area of the $LaNiO_3$, and the d=0.381 nm (101) crystal plane of adjacent areas. FIG. 3c displays the parallel fringes of the d=0.273 nm (110) crystal plane of $LaNiO_3$ in other areas [20,21]. The Fast Fourier Transform (FFT) [22] image (FIG. 3d) shows two different distances of 0.005 and 0.007 1/pm corresponding to the (101) and (110) crystal planes of $LaNiO_3$. These results are consistent with the HRTEM micrographs.

FIG. 4 presents the nitrogen absorption and desorption isotherms for the $LaNiO_3$. The BET surface area of the $LaNiO_3^{-3}$ is 37.67 $m^2g^{-1}$. The pore diameter distribution of the hierarchical $LaNiO_3^{-3}$ was measured by the Barret-Joyner-Halenda(BJH) method and is shown in the insets of FIG. 4. The pore size calculated by the adsorption branch is in the range of 100-110 nm. The present hierarchical $LaNiO_3^{-3}$ sphere with nanosheets will potentially exhibit superior performance in catalysis properties.

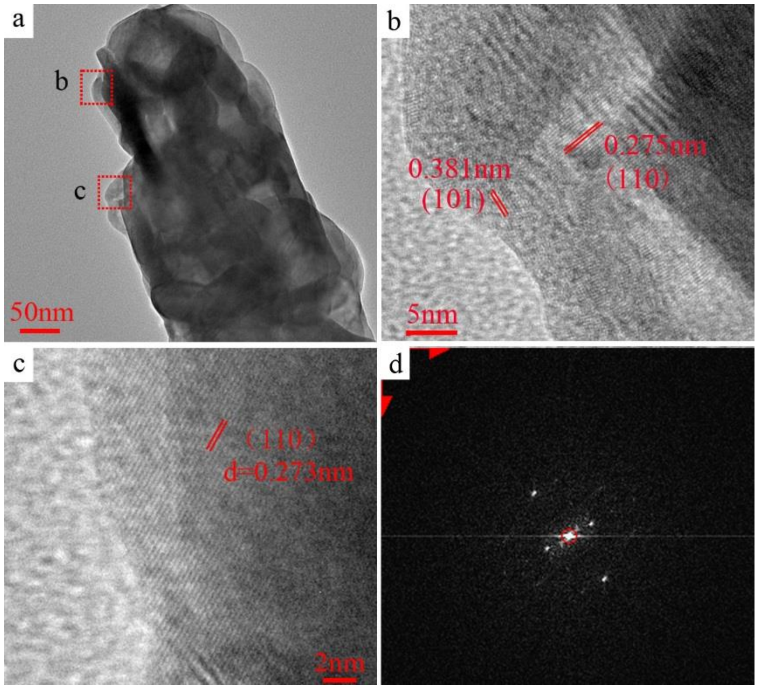


FIG. 3a. **TEM urchin-flowerlike hierarchical $LaNiO_3$ spheres, (b, c) HRTEM micrographs and (d) FFT image.**

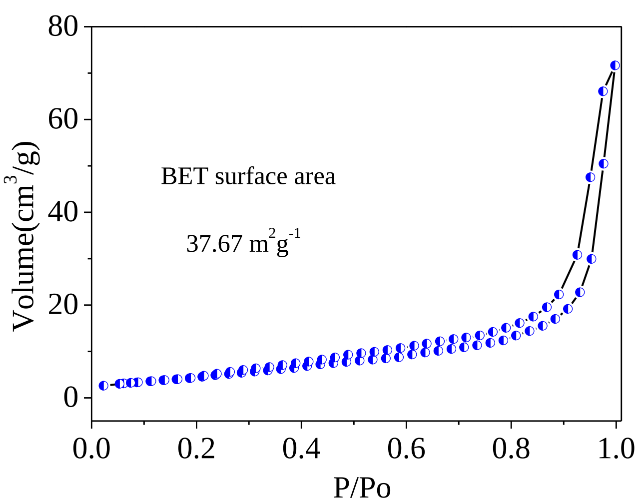


FIG. 4. **Nitrogen physisorption isotherms spectra of urchin-flowerlike hierarchical $LaNiO_3^{-3}$ spheres.**

### X-ray photoelectron spectroscopy analysis

The corresponding XPS spectra provide further structural information on the obtained urchin-flowerlike hierarchical $LaNiO_3$ spheres. The spectra of all element valence bands for the $LaNiO_3$ spheres are shown in FIG. 4. FIG. 4a shows that the sample contains elemental La, Ni, O, C, and S. The C and S were introduced via the surfactant (SDBS). In FIG. 4b, the C 1s spectrum consists of a single peak with a binding energy of 285.62 eV. In FIG. 4c, the La 3d spectrum [23,24] consists of two individual peaks at 837.67 and 854.89 eV, which can be attributed to the La $3d_{5/2}$ and La $3d_{3/2}$ binding energies, respectively. The binding energies of La $3d_{5/2}$ and La $3d_{3/2}$ are larger than the standard values (La $3d_{5/2}$ 836.0 eV; La $3d_{3/2}$ 853.0 eV) [25-26]. Furthermore, the La 3d peaks are shifted by 1.6 eV toward the larger binding energies because of the La-Ni interaction.

In FIG. 4d, the Ni 2p spectra [27-28] of the $LaNiO_3$ consist of four relevant peaks at 860.13 and 868.09 eV and 851.31 and 855.18 eV, which can be attributed to the Ni $2p_{1/2}$ and Ni $2p_{3/2}$ binding energies, respectively. The binding energies of Ni $2p_{1/2}$ and Ni $2p_{3/2}$ are lower than the standard values (Ni $2p_{1/2}$ 869.29 eV; Ni $2p_{3/2}$ 852.6 eV) [29-30]. The Ni 2p peak centered at 855.18 eV indicates the possible presence of $Ni(OH)_2$. However, the decomposition temperature of $Ni(OH)_2$ ranges from 200 to 300°C and therefore $Ni(OH)_2$ does not exist in the $LaNiO_3$ spheres that were calcined at 750°C for 5.5 h. Additionally, it should be noted that the Ni 2p peaks are shifted by 1.2 eV toward lower binding energies because of the La-Ni interaction [31]. The change in electron binding energy occurs primarily because of the formation of LaNiO3microspheres. These results indicate that the chemical state of $LaNiO_3$ is the same in the support.

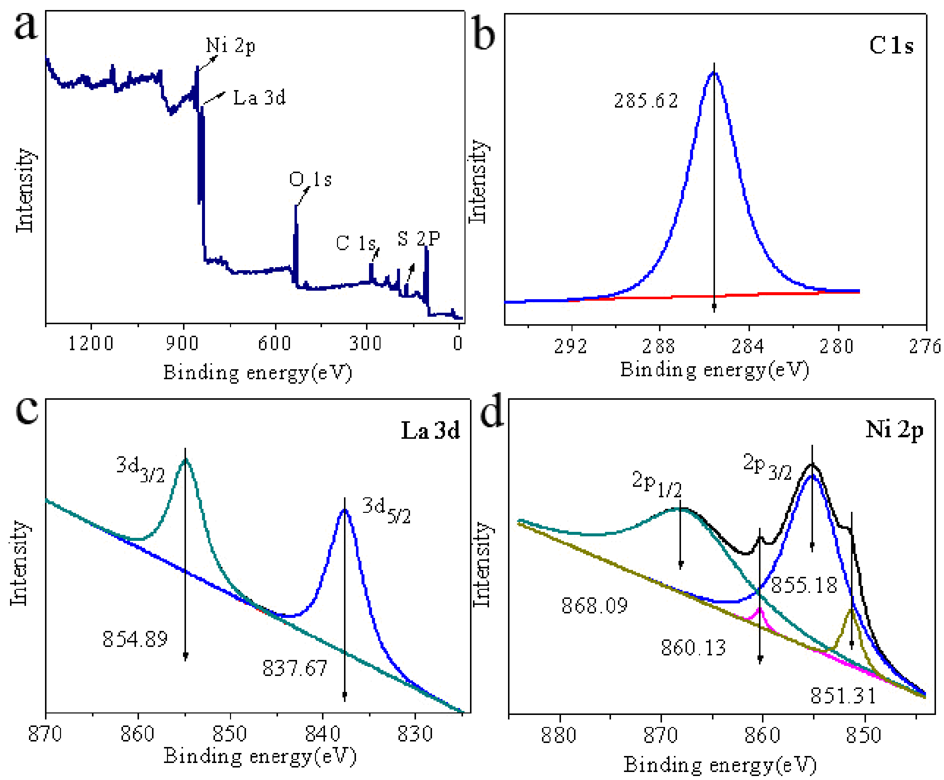


FIG. **5 XPS spectra of urchin-flowerlike hierarchical $LaNiO_3^{-3}$ spheres.**

**Temperature-programmed reduction analysis**

$H_2$-TPR experiments were conducted to investigate the relative reducibility of urchin-flowerlike hierarchical $LaNiO_3^{-3}$ spheres with different La/Ni molar ratios. FIG. 6 shows the TPR profiles of the $LaNiO_3$ spheres. The $LaNiO_3$ spheres had three main reduction peaks around 350°C (Tr1), 500°C(Tr2), 680 °C(Tr3). Concerning the peak area, the second (reduction desk) and third peaks of $LaNiO_3^{-3}$ are much higher than those of $LaNiO_3^{-1}$, $LaNiO_3^{-2}$ and $LaNiO_3^{-4}$ while those for the second peaks are not clear. According to Zeng GM [32] the reduction of $LaNiO_3$ proceeds in three steps:

$4\ LaNiO_3+2\ H_2 \rightarrow La_4Ni_3O_{10}+Ni+2\ H_2O$ (250-360°C) (1)

$La_4Ni_3O_{10}+3\ H_2 \rightarrow La_2NiO_4+2\ Ni+La_2O_3+3\ H_2O$ (360-430°C) (2)

$La_2NiO_4+H_2 \rightarrow Ni+La_2O_3+H_2O$ (600-750°C) (3)

The TPR results shown in FIG. 6 demonstrate that several kinds of Ni species present on the catalyst surface. As revealed, the first peak is attributed to the crystalline phases and to the successive reduction of $LaNiO_3$ to $La_4Ni_3O_{10}$ and $Ni^0$ (Tr1). And the second peak is attributed to the crystalline phases and to the successive reduction of $La_4Ni_3O_{10}$ to $La_2NiO_4$, $La_2O_3$ and $Ni^0$ (Tr2). For the third peak, they should be ascribed to the reduction of $La_2NiO_4$ incorporated into the $La_2O_3$ and $Ni^0$ (Tr3), in good agreement with $LaNiO_3$ reported previously [33]. In addition, the three peaks reveal that the urchin-flowerlike hierarchical $LaNiO_3$ sphere materials had a significant impact on the reducibility.

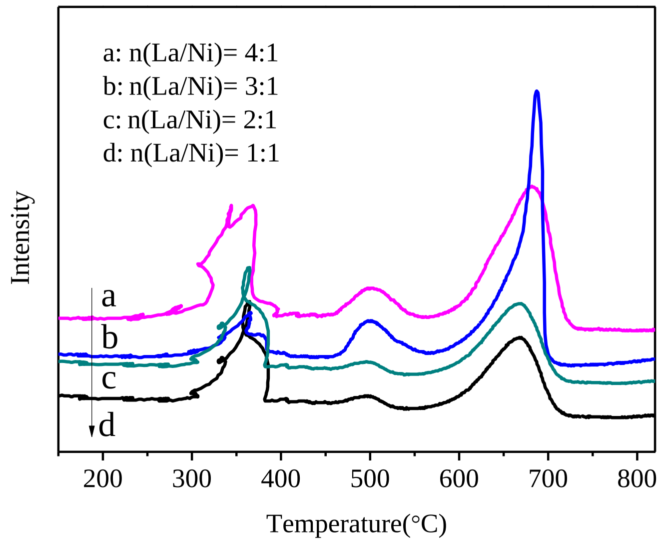


FIG. 6. **TPR spectra of urchin-flowerlike hierarchical a: $LaNiO_3^{-4}$; b: $LaNiO_3^{-3}$; c: $LaNiO_3^{-2}$; d: $LaNiO_3^{-1}$ spheres.**

**Catalytic activity of $LaNiO_3$ spheres**

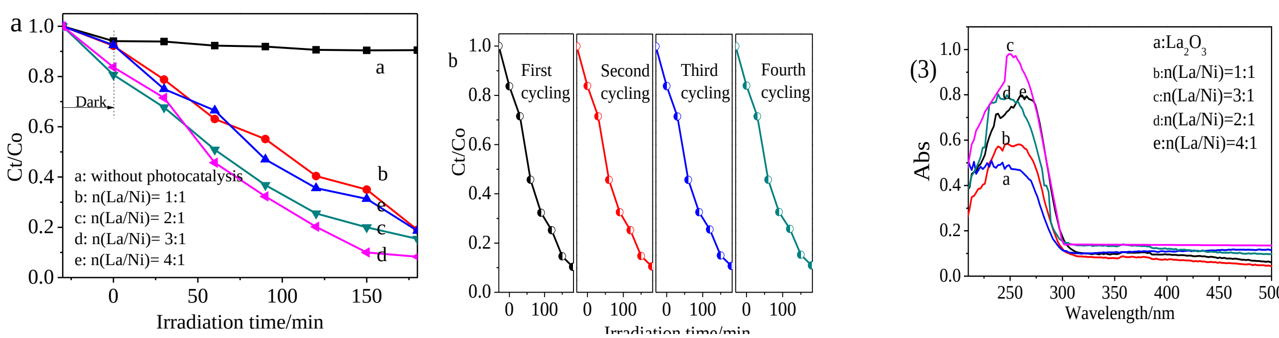


FIG.7. **Degradation curves and UV-Vis DRS spectra of urchin-flowerlike hierarchical $LaNiO_3$ spheres.**

FIG. 7(1) displays the RB degradation activity of different urchin-flowerlike hierarchical $LaNiO_3$ spheres by plotting Ct/Co as a function of time [34]. Here Co and Ct are the initial concentration and concentration of RB at time, respectively. As shown in FIG. 7(1) a, RB degradation without a photo catalyst was also performed, and the results demonstrated that the degradation of RB was very slow in the absence of a photo catalyst under ultraviolet-light irradiation. As shown in FIG. 7(1), in the presence of hierarchical $LaNiO_3$ spheres but in darkness, the removal rate of RB was 18% within 30 min. Almost no change occurred during the 30 min, which was attributed to the low specific surface area of the samples. All change occurred during the next 270 min, which was attributed to good photocatalytic activities of $LaNiO_3$. It can be seen 95.63% of the RB was degraded by $LaNiO_3^{-3}$ spheres under identical conditions, but under irradiation with ultraviolet light. This demonstrated that the hierarchical $LaNiO_3^{-3}$ sphere nanostructures exhibited excellent in situ ultraviolet-light-driven photocatalytic performance.

Moreover, the regeneration capability of the hierarchical $LaNiO_3^{-3}$ spheres was examined for degradation of dye during a four-cycle experiment, which was very important for the hierarchical $LaNiO_3^{-3}$ spheres to apply in environmental technology. FIG. 7(2) shows the plot of degradation percentage as a function of cycle number. As shown in FIG. 7(2), each experiment was carried out under identical conditions; after a four-cycle experiment, the photocatalytic activity of the hierarchical $LaNiO_3^{-3}$ spheres remained almost unchanged. It was indicated that the hierarchical $LaNiO_3$ spheres displayed an efficient photoactivity for the degradation of organic pollutants under ultraviolet-light irradiation and could easily be separated for reuse.

FIG. 7(3) shows the absorbance vs. wavelength plots for urchin-flowerlike hierarchical $LaNiO_3$ spheres. It is interesting to note that the absorption spectra show a distinct broad feature at 300 nm for the $LaNiO_3$ spheres. The absorption peaks indicate the zero dimensional characteristics of corresponding samples, with the lower wavelength absorption feature is assigned to the size-quantized particles.

## Conclusion

In summary, the modified coprecipitation method has been used to produce urchin-flowerlike hierarchical $LaNiO_3$ spheres. This approach provides a relatively simple, environmentally friendly, economical method that is suitable for large-scale production and is affordable for the preparation of magnetic microspheres with a tunable diameter range of 20 μm to 30 μm. Furthermore, we report here another important finding on the urchin-flowerlike hierarchical $LaNiO_3$ spheres as a catalyst for MB degradation with high degradation efficiency.

## REFERENCES


1. Rout A, Wellens S, Binnemans K. Separation of rare earths and nickel by solvent extraction with two mutually immiscible ionic liquids. RSC Adv. 2014;4:5753-8.
2. Gao ZJ, Kang L, Luo YC. Microstructure and electrochemical hydrogen storage properties of La-R-Mg-Ni-based alloy electrodes. New J Chem. 2013;37:1105-14.
3. Wang WY, Yang YQ, Luo H, et al. Effect of La on Ni-W-B Amorphous Catalysts in Hydrodeoxygenation of Phenol. Ind Eng Chem Res. 2011;50:10936-42.
4. Benjaram, Reddy M, Katta L, et al. Novel Nanocrystalline $Ce_{1-x}LaxO_{2-\delta}$ (x=0.2) Solid Solutions: Structural Characteristics and Catalytic Performance. Chem Mater. 2010;22(2):467-75.
5. Zou YC, Luo Y, Wen N, et al. Fabricating $BaZrO_3$ hollow microspheres by a simple reflux method. New J Chem. 2014;38:2548-53.
6. Shanmugasundaram A, Basak P, Manorama SV, et al. Hierarchical Mesoporous In $2O_3$ with Enhanced CO Sensing and Photocatalytic Performance: Distinct Morphologies of $In(OH)_3$ via Self Assembly Coupled in Situ Solid−Solid Transformation. ACS Appl Mater Interfaces. 2015;7 (14):7679-89.

7. Yang Y, Tian CG, Sun L, et al. Facile Synthesis of Novel 3D Nanoflower-Like $Cu_xO$/Multilayer Graphene Composites for Room Temperature $NO_x$ Gas Sensor. Nanoscale. 2014;6:7369-78.
8. Woolley RJ, Illy BN, Ryan MP, et al. In situ determination of the nickel oxidation state in $La_2NiO_{4+\delta}$and $La_4Ni_3O_{10-\delta}$using X-ray absorption near -edge structure. J Mater Chem. 2011;21:18592-6.
9. Aguadero A, Alonso JA, Martı´nez-Lope MJ, et al. In situ high temperature neutron powder diffraction study of oxygen-rich $La_2NiO_{4+\delta}$ in air: correlation with the electrical behavior. J Mater Chem. 2006; 16:3402–8.
10. Li P, Sun MY, Bai HL. Fabrication of fully epitaxial ZnO/$Fe_3O_4$ heterostructures on conductive $LaNiO_3$. J Thin Solid Films. 2012;520:5971-6.
11. Peng EW, Ding J, Xue JM. Concentration-dependent magnetic hyperthermic response of manganese ferrite-loaded ultrasmall graphene oxide nanocomposites. New J Chem. 2014;38:2312-19.
12. Dong RH, Liu WM, Hao JC. Soft Vesicles in the Synthesis of Hard Materials. ACS Acc Chem Research. 2012;45(4):504-13.
13. Tian F, Zhu J, Wei D. Fabrication and Magnetism of Radial-easy-magnetized Ni Nanowire Arrays. J Phys Chem C. 2007;111:12669-72.
14. Rajesh JA, Pandurangan A. Tunable filling rate and increased ferromagnetic properties of nickel-filled carbon nanotubes synthesized from a Pauli paramagnetic lanthanum nickel ($LaNi_5$) alloy catalyst. J Mater Chem C. 2013;1:6996-7008.
15. Joswig JO, Lorenz T, Seifert G. The virtues of magnetism. ACS Nano. 2013;7(12):10449-51.
16. Kafizas A, Parkin IP. Inorganic thin-film combinatorial studies for rapidly optimising functional properties. Chem Soc Rev. 2012;41:738-81.
17. Odedairo T, Zhou W, Chen JL, et al. Flower-like perovskite $LaCr_{0.9}Ni_{0.1}O_{3-\delta}$-NiO nanostructures: a new candidate for $CO_2$ reforming of methane. RSC Adv. 2014;4:21306-12.
18. Xie D, Su QM, Yuan WW, et al. Synthesis of porous NiO-wrapped graphene nanosheets and their improved lithium storage properties. J Phys Chem C. 2013;117:24121-28.
19. Wang MH, Chen S, Xia Y, et al. Nanoassemblies of colloidal gold nanoparticles by oxygen-induced inorganic ligand replacement. Langmuir. 2010;26:9351-6.
20. Pan JH, Huang QZ, Koh ZY, et al. Scalable synthesis of urchin-and flowerlike hierarchical NiO microspheres and their electrochemical property for lithium storage. ACS Appl Mater Interfaces. 2013;5:6292-9.
21. Kundu J, Pradhan D. Controlled synthesis and catalytic activity of copper sulfide nanostructured assemblies with different morphologies. ACS Appl Mater Interfaces. 2014;6:1823-34.
22. Gao GG, Song CY, Zong XM, et al. Solvent-controlled 3D lanthanide-polyoxometalate frameworks: Reduction and stabilization of Ag nanocomposites and catalytic properties. Cryst Eng Comm. 2014;16:5150-8.
23. Yan HJ, Tian CG, Sun LB, et al. Small-sized and high-dispersed WN from $[SiO_4(W_3O_9)_4]^{4-}$ clusters loading on GO-derived graphene as promising carriers for methanol electro-oxidation. Energy Environ Sci. 2014;7:1939-49.
24. Huang Z, Wang XG, Wang ZY, et al. High catalytic performance and sustainability of the Ni/$La_2O_3$ catalyst for daily pre-reforming of liquefied petroleum gas under a low steam/carbon molar ratio. RSC Adv. 2014;4:14829-32.
25. da Silva AAA, Costa LO, Mattos LV, et al. The study of the performance of Ni-based catalysts obtained from $LaNiO_3$ perovskite-type oxides synthesized by the combustion method for the production of hydrogen by reforming of ethanol. Catal Today. 2013;213:25-32.

26. Chroneos A, Parfitt D, Kilner JA, et al. Anisotropic oxygen diffusion in tetragonal $La_2NiO_{4+d}$: molecular dynamics calculations. J Mater Chem. 2010;20:266-70.
27. Addato S D, Grillo V, Altieri S, et al. Assembly and fine analysis of Ni/MgO core/shell Nanoparticles. J Phys Chem C. 2011;115:14044-9.
28. Radu T, Benea D, Lucacel RC, et al. X-ray Photoelectron spectroscopic characterization of Ag nanoparticles embedded bioglasses. J Phys Chem C. 2012;116:17975-9.
29. Yi HH, Yu QF, Tang XL, et al. Phosphine adsorption removal from yellow phosphorus tail gas over CuO-ZnO-$La_2O_3$/activated carbon. Ind Eng Chem Res. 2011;50:3960-5.
30. Li GS, Zhang Y, Wu L, et al. An efficient round-the-clock $La_2NiO_4$ catalyst for breaking down phenolic pollutants. RSC Adv. 2012;2:4822-8.
31. Ramana CV, Vemuri RS, Kaichev VV, et al. X-ray Photoelectron spectroscopy depth profiling of $La_2O_3$/Si thin films deposited by reactive magnetron sputtering. ACS Appl Mater Interfaces. 2011; 3:4370-3.
32. Zeng GM, Shao JJ, Gu RX, et al. Facile fabrication of a highly active shell-core LaNi(Mg, Al)O 3 @Mg–Al catalyst for ethanol steam reforming. Catalysis Today. 2014;233(15):31-7.
33. Hou YC, Ding MW, Liu SK, et al. Ni-substituted $LaMnO_3$ perovskites for ethanol Oxidation. RSC Adv. 2014;4:5329-38.
34. Zhang ZY, Shao CL, Li XH, et al. Electrospun nanofibers of p-Type NiO/n-Type ZnO Heterojunctions with enhanced photocatalytic activity. ACS Appl Mater Interfaces. 2010;2(10):2915-23.